Bima Journal of Science and Technology, Vol. 8(3) Sept, 2024 ISSN: 2536-6041

DOI: 10.56892/bima.v8i3A.802

Determination of Elastic Properties of Overburden Materials Using Intercept Time of Seismic Refraction in Ayede, South-Western Nigeria

Femi Emmanuel Ikuemonisan[1]*, Taiwo Joshua Aluko[2], Yusuf Olanrewaju Kayode[3], Anthony Segara Ajose[4] and Sakiru Abiodun Okedeyi[5]

[1,3,4,5]Department of Physics, Lagos State University of Education, Lagos, Nigeria

[2]Chrisland University, Abeokuta, Ogun State, Nigeria

Corresponding Author: ikuemonisanfe@lasued.edu.ng

ABSTRACT

This study investigates the elastic properties of overburden materials in Ayede, South-Western Nigeria, using the seismic refraction intercept time method. Seismic survey was conducted to obtain velocity profiles, which were then used to compute elastic parameters, including Young's modulus, shear modulus, and Poisson's ratio for the respective layers. The study reveals a stratigraphic progression from unsaturated sand at the surface to saturated tar sand, and finally to dense marl. The first layer, consisting of unsaturated sand, extends to a depth of 6.70 meters with a primary wave velocity (V_p) of 803 m/s, secondary wave velocity (V_s) of 305 m/s, and a density of 1650 kg/m³. The elastic properties include a bulk modulus of 0.859 x 10^9 N/m² and a shear modulus of 0.154 x 10^9 N/m². The second layer, comprising saturated tar sand, reaches a depth of 11.9 meters with a V_p of 1898 m/s, V_s of 737 m/s, and a density of 2045 kg/m³, yielding a bulk modulus of 5.886 x 10^9 N/m² and a shear modulus of 1.111 x 10^9 N/m². The final marl layer, the densest, exhibits a V_p of 3300 m/s, V_s of 1091 m/s, a bulk modulus of 21.55 x 10^9 N/m², and a shear modulus of 2.796 x 10^9 N/m².

Keywords: Elastic properties; Intercept time; Marl; Overburden layer; Seismic refraction.

INTRODUCTION

Seismic refraction is a geophysical method widely used to investigate subsurface characteristics by analyzing the travel times of seismic waves refracted at geological boundaries (Cox et al., 2020; Syukri et al., 2020; Pegah & Liu, 2016; Fadhli et al., 2022). This technique is particularly valuable in determining the elastic properties of overburden materials, which are fundamental for various engineering and environmental applications (Uhlemann et al., 2016; Akingboye & Ogunyele, 2019, Imani et al., 2021). The overburden layers, usually composed of unconsolidated materials like soil, sand, and gravel, overlay bedrock and significantly influence the mechanical behavior and stability of the near-surface environment (Conway-White et al., 2022; Ullah et al., 2023). These materials are termed unconsolidated because their loosely packed particles lack the cohesion or cementation needed to form a solid structure (Malehmir et al., 2016; Kaunda, 2021; Gago et al., 2022; Ullah et al., 2023).

Ayede, located in Southwestern Nigeria, features a unique geological setting with diverse lithological formations, which makes a comprehensive understanding of its subsurface properties essential. This understanding is particularly important for accurately determining the elastic properties of overburden materials, which is fundamental for evaluating ground suitability for construction projects (Zhu et al., 2022; Tokgozoglu et al., 2023) and ensuring the safety and stability of infrastructure (Olusola, 2021). Moreover, knowledge of these properties enhances environmental studies by providing detailed information on soil and groundwater characteristics, which are vital for sustainable land use and resource management (Abd El Aal & Rouaiguia, 2020; Falowo, 2023; Rana et al., 2023).

DOI: 10.56892/bima.v8i3A.802

Additionally, this understanding supports mineral exploration by delineating subsurface structures and identifying potential mineral deposits (Nogueira et al., 2016; Brixová et al., 2018).

Previous studies in similar geological settings have primarily focused on the general characterization of subsurface layers and the identification of major geological boundaries (Ozebo & Ikuemonisan, 2019; Adewoyin et al., 2021; Balogun et al., 2023; Alabi et al., 2023). While these investigations have provided valuable baseline data, they often lacked detailed analysis of the elastic properties of overburden materials. Specifically, there has been a notable gap in the application of the intercept time method (ITM) of seismic refraction for this purpose in Ayede. Moreover, previous studies have not comprehensively addressed the variations in elastic properties within the overburden, which are important for understanding site-specific ground behavior.

In addressing this gap, the study determined the elastic properties of overburden materials in Ayede using the intercept time method of seismic refraction. These materials, comprising unconsolidated layers of soil, and sand, lie above the bedrock. Seismic refraction surveys conducted across the study area provided detailed velocity profiles, enabling the calculation of key elastic parameters, including Young's modulus, shear modulus, and Poisson's ratio. This approach offers a higher resolution of subsurface properties than previously available studies. The findings deliver critical information for geotechnical assessments, resource exploration, and environmental management in Ayede.

MATERIALS AND METHODS

Study Area

The study area is centered at latitude 6.5622600°N and longitude 4.5430400°E (Figure 1), with an elevation of about 45 meters above sea level. It is located within the Waterside area of Ogun State, Southwestern Nigeria. Ogun State is bordered by Benin Republic to the west, Lagos State to the south, Oyo and Osun States to the north, and Ondo State to the east. The region is underlain by sedimentary rocks of the Abeokuta Formation, overlying the basement complex (Ajayi et al. 2022; Eludoyin et al., 2023). The region is further overlaid by the Ewekoro, Shosun, and Ilaro Formations, capped by the coastal plain of sand (Adediran et al., 1991). The sedimentary rocks in Southwestern Nigeria are part of the Dahomey Embayment, extending from Volta, Ghana, through the Republic of Benin to the Okitipupa Ridge (Mosuro et al. 2021; Adamolekun et al., 2022). The Sagamu Formation, a massive bioclastic Paleocene carbonate rock, is exposed in the Sagamu and Ewekoro areas along the Gulf of Guinea's continental margins (Nton & Adeyemi, 2015; Oluwajana et al., 2021). The area's notable geological features include tar sand, kaolin, bitumen, natural gas, and other hydrocarbon deposits.

Bima Journal of Science and Technology, Vol. 8(3) Sept, 2024 ISSN: 2536-6041

DOI: 10.56892/bima.v8i3A.802

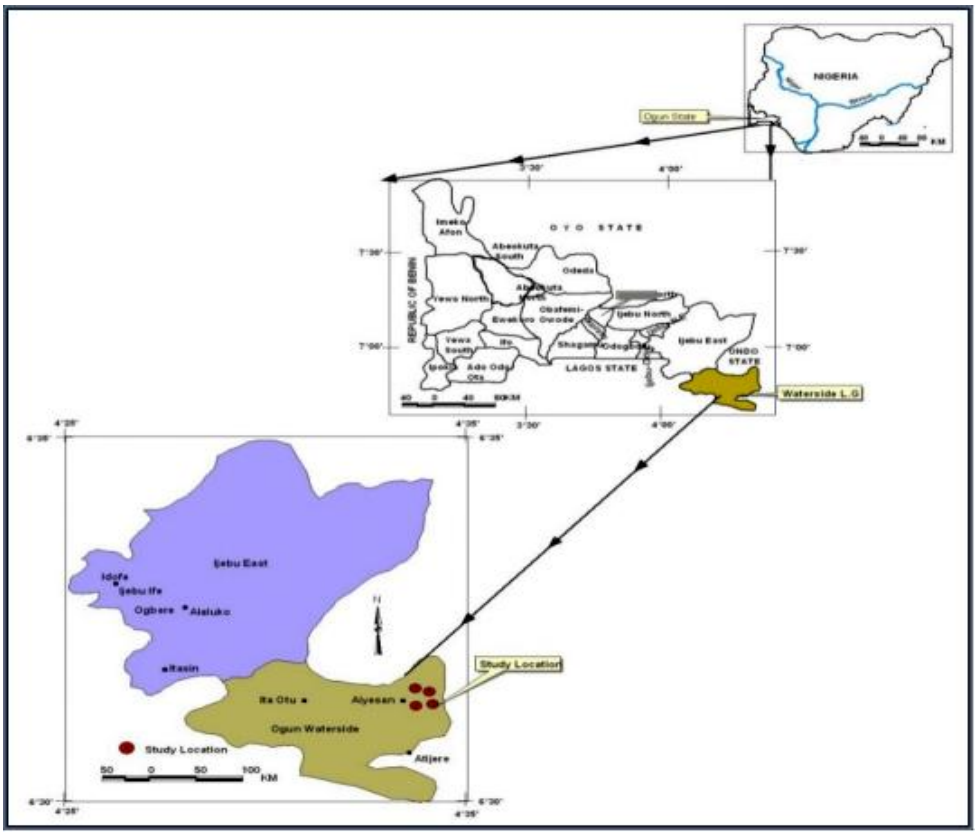

Figure 1: Location of the study area

Theoretical Background

The seismic refraction method is a geophysical technique used to investigate subsurface properties by analyzing the travel time of seismic waves refracted at the boundaries between different geological layers (Alhassan et al., 2010; Crutchley & Kopp, 2018). This method involves generating seismic waves using a hammer strike as a controlled source and recording the arrival times of these waves at an array of geophones placed on the surface (Imani et al., 2021; Aisyah et al., 2022). When seismic waves encounter a boundary between materials with different seismic velocities, they bend, or refract, according to Snell's Law (Wang et al., 2021). By measuring the travel times of these refracted waves, geophysicists can determine the velocity structure of the subsurface, which in turn provides information about the composition, thickness, and depth of the various geological layers (Griffiths & King, 2013; Sunkpal et al., 2022). Seismic refraction is commonly used in engineering, environmental studies, and exploration geophysics to map bedrock topography, detect subsurface voids, and assess soil and rock properties (Nyquist et al., 1996; Kearey, Brooks, & Hill, 2002; Reynolds, 2011; Uecker et al., 2023). The key concept is that seismic rays bend when they strike a geological boundary at a certain angle (Maunde & Bassey, 2017; Mengjia et al., 2024). The degree of bending, θ_2, is determined by the velocities of the two geological layers, V_1 and V_2, and the angle of incidence, θ_1, as described by Snell's Law:

$$\frac{\sin\theta_1}{\sin\theta_2} = \frac{V_1}{V_2} \qquad (1)$$

When the velocity of the upper layer is lower than that of the lower layer, the refracted angle increases as the incident angle rises, eventually reaching 90^0. At this point, the refracted wave travels along the boundary between the two layers. Estimating near-surface layers using seismic refraction has long been an area of significant interest. In this study, we utilized a 12-channel signal enhancement seismograph, geophones, a sledgehammer, and a metal plate

DOI: 10.56892/bima.v8i3A.802

to generate seismic waves. Additional equipment included measuring tape, extension cables, a battery, a switch, and a global positioning system. The electromagnetic geophones, which made direct contact with the ground, converted the seismic energy from the source into electrical voltage, which depends on velocity. Both the geophones and the seismic energy source (sledgehammer) were firmly in contact with the soil. The waves detected by the geophones were recorded by the seismograph, which was connected to the geophones. The multi-channel seismograph recorded the seismic waveforms simultaneously, allowing us to observe data trends and reliably identify the first arrival times of P-waves and the corresponding S-wave arrival times for each geophone. The seismic energy was generated by striking a plate with a sledgehammer four times, using the signal enhancement capabilities of the seismograph. A timing signal at the moment of impact ($t = 0$) was sent to the seismograph, with the impact time detected by a mechanical switch (piezoelectric device) on the geophone.

Materials Used

Equipment and tools

The primary instruments used in this survey were geophones, sledgehammers, seismographs, and ancillary tools such as measuring tapes and GPS devices. Geophones played a crucial role in this survey, as they were responsible for detecting seismic waves traveling through the subsurface. High-sensitivity geophones were chosen for their ability to capture even the slightest ground vibrations. These sensors were strategically placed at regular intervals of 5 to 10 meters along the survey line, ensuring comprehensive coverage of the study area. A sledgehammer and a metal plate were employed to generate the seismic waves needed for the survey. The sledgehammer was struck against the metal plate placed on the ground, creating consistent and controllable seismic energy. This method was chosen for its simplicity and effectiveness in producing reliable seismic waves. The generated waves traveled through the subsurface layers, refracting at various interfaces before being detected by the geophones.

Recording the travel times of these seismic waves was facilitated by a high-precision seismograph. This instrument, equipped with multiple channels, allowed for the simultaneous recording of data from all the geophones. The seismograph ensured accurate and reliable data acquisition, which was critical for the subsequent analysis. Additionally, measuring tapes and stakes were used to establish the survey line and accurately position the geophones. The measuring tape enabled precise spacing between geophones, while the stakes marked their positions along the line. A GPS device was also utilized to record the exact coordinates of the survey line and each geophone position. This geospatial information was crucial for correlating the seismic data with specific locations in the study area, enhancing the accuracy and relevance of the findings.

Software

The data collected during the survey were analyzed using *SmartRefract* software designed for seismic refraction analysis. This software facilitated the plotting of travel times against distances, calculating apparent velocities, and interpreting subsurface layer properties. The theoretical background, which supports the use of this software, is provided in Section 3.5. In addition to the seismic refraction analysis software, Quantum Geographic Information System (QGIS) was employed to map the layout of the study area.

Seismic Data Analysis and Interpretation

ITM assumes that subsurface material layers or zones are present, with each layer having a uniform velocity (Rucker, 2002; Alaminiokuma, 2020). Lateral velocity changes, especially in shallow subsurface profiles, are detected by interpreting data between adjacent shot points as smaller, shorter seismic lines (Çakır & Coşkun, 2021). Velocities are determined by analyzing the slopes of the time-offset plot of the first seismic signal arrivals at various geophone locations, calculated as distances traveled

DOI: 10.56892/bima.v8i3A.802

divided by time elapsed for each segment of the plot (Silahtar et al., 2020). A minimum of three data points is needed to confidently interpret each velocity slope. Interfaces between different velocity material zones are assumed to be planar, and depth interpretation formulas are used to calculate the depths of these interfaces (Washima et al., 2020). Travel time data at each geophone is plotted as a graphical relationship between geophone numbers and travel time. The velocities of P-waves and S-waves, as well as the thickness of each layer at the four locations, were calculated based on intercept time graphic data.

Field Procedure

We utilized the seismic refraction method to determine the elastic properties of overburden materials. This technique involves generating seismic waves and measuring their travel times through the subsurface to infer the properties of underlying materials. First, a survey line was established across the study area. Geophones, which are sensors used to detect seismic waves, were placed at regular intervals of 10 meters along this line. This spacing ensures comprehensive coverage and accurate data collection across the entire area of interest. A sledgehammer was employed as the seismic energy source. Initially, the source was positioned at the beginning of the geophone line, and in subsequent stages, it was moved to multiple points along the line to improve the accuracy and resolution of the data. The sledgehammer was struck against a metal plate placed on the ground to generate seismic waves. These waves propagated through the subsurface and were refracted at interfaces where there were changes in material properties, such as different soil and rock layers.

As the refracted waves traveled back to the surface, they were detected by the geophones. A seismograph was used to record the travel times of these waves from the source to each geophone. The recorded travel times were then plotted against the distances from the source to each geophone, resulting in a time-distance graph. The initial straight-line segments of this graph indicated the apparent velocities of the subsurface layers. By analyzing the slopes of these segments, we could determine the velocities at which seismic waves traveled through different materials. Using the intercept times from the graph and the calculated apparent velocities, we computed the thickness and elastic properties of the overburden materials. These calculations were based on standard equations and interpretation techniques commonly used in seismic refraction analysis (Sheriff & Geldart, 1995).

Parameter Estimation

Determination of P-wave and S-wave velocities

Determining P-wave (primary wave) and S-wave (secondary wave) velocities is essential for assessing the elastic properties of overburden materials. These velocities reveal the mechanical behavior and composition of the subsurface layers. The intercept time is connected to both the thickness and velocity of geological layers on either side of an interface. Accurately determining this value is crucial for making reliable estimates of the depths of geological interfaces and other related parameters. When the travel time (t) recorded from the seismograph is plotted against the source-detector distance (x) for the first layer, the relationship between t and x is expressed as:

$$t_{direct} = \frac{x}{v_1} \qquad (2)$$

Where, x = distance from source to receiver, V_1 is the velocity of the first or uppermost layer. The slope $\frac{1}{v_1}$ was evaluated to obtain the velocity of the first layer as v_1.

$$t_{refracted1} = \frac{x}{v_2} + 2h_1\sqrt{\frac{1}{v_1^2} - \frac{1}{v_2^2}} \qquad (3)$$

DOI: 10.56892/bima.v8i3A.802

h_1 Thickness of the first layers, V_2 is the velocity of the second layer, x and h_1 are the same as in the direct ray equation. Equation (3) was used to determine the slope $\frac{1}{v_2}$ and the depth h_1 of the first layer. The value of v_2 was then evaluated from the slope travel time-offset plot for the four seismic shot points.

For the third layer, $t_{refracted2} = \frac{x}{v_3} + 2h_1\sqrt{\frac{v_3^2 - v_2^2}{v_3^2 v_1^2}} + 2h_2\sqrt{\frac{v_3^2 - v_2^2}{v_3^2 v_2^2}}$ (4)

We have $\frac{1}{v_3}$ as the slope and the value of v_3 which is the velocity of the third layer was determined in the plot of P-wave and S-wave.

Depth determination

The intercept time $t_{int} = 2h_1\sqrt{\frac{1}{v_1^2} - \frac{1}{v_2^2}}$ (5)

This gives:

$$h_1 = \frac{t_{int1}}{2\sqrt{\frac{1}{v_1^2} - \frac{1}{v_2^2}}} \quad (6)$$

h_1 is the thickness of the first layer, t_{int1} is the intercept on travel time axis for the first refraction. For the second layer, $h_2 = \frac{t_{int2} - t_{int1}}{2\sqrt{\frac{1}{v_2^2} - \frac{1}{v_3^2}}}$ (7)

where h_2 *is the* thickness of the second layer, and t_{int2} is the intercept on traveltime axis for the second refraction. Though three layers were detected, but only thickness of the first two layers can be estimated because the second refracted ray travels along the top of third layer cannot be calculated based on the available data.

Elastic properties

Gardner et al. (1974) conducted a series of empirical studies and established the following relationship between P-wave and density:

$$\rho = av^{1/4} \quad (8)$$

Where ρ = density in g/cm^3, $a = 0.31$ when v *is* in m/s and is 0.23 when V is in ft/s. The elastic properties for each layer were calculated using equation (8) and the relationship between elastic constants and seismic velocities described by Sheriff and Geldart (1995).

Parameter definition

Density (ρ): Refers to the mass per unit volume of the soil or rock. For soils, it helps determine compaction and load-bearing capacity, while in rocks, it can indicate the type and porosity.

Poisson's Ratio (σ): Indicates how the soil or rock deforms in directions perpendicular to the applied stress. For soils, it helps in understanding how soil will expand or contract laterally when compressed. In rocks, it provides insight into how the material will behave under stress, particularly in geological engineering.

Bulk Modulus (k): Measures the resistance of soil or rock to uniform compression. For soils, it reflects how the volume changes under pressure,

DOI: 10.56892/bima.v8i3A.802

which is important for understanding soil compaction and settlement. For rocks, it helps in assessing their compressibility and ability to withstand pressure.

Shear Modulus (μ): Describes the resistance of soil or rock to shear stress, which is crucial for understanding how these materials deform under shear forces. For soils, it relates to stability and load-bearing capacity. For rocks, it indicates how they will respond to forces causing sliding or shearing.

Lame Constant (λ): Used in conjunction with the shear modulus to describe elastic behavior in soils and rocks. It helps relate stress and strain in these materials, aiding in the analysis of their deformation under various loading conditions.

Young's Modulus (E): Measures the stiffness of soil or rock, indicating how much they will deform under axial loads. For soils, it is important for predicting settlement and structural load responses. For rocks, it reflects their ability to resist deformation under stress.

RESULTS AND DISCUSSION

Determining the type of lithology composition in the subsurface based solely on velocity values is challenging because different materials may have overlapping velocity ranges. However, with the knowledge of the elastic properties of various rock samples combined with their velocities, it is possible to practically deduce the type of geologic formation with minimal error (George et al., 2010). Therefore, in addition to identifying the lithology compositions of the study areas using measured P-wave and S-wave velocities, the elastic properties of the subsurface materials were also determined to draw inferences. Table 1 shows the details of the subsurface layers at seismic shot point A. As can be seen in Table 1, the stratigraphic profile at seismic shot point A reveals a sequence starting with loose, unsaturated sand at the surface, transitioning to more compact, fluid-filled tar sand, and finally reaching a dense and rigid marl layer. The increasing velocities, densities, and elastic moduli with depth reflect a transition from unconsolidated to highly consolidated materials. The first layer, which consists of unsaturated sand, reaches down to a depth of 6.70 meters.

Table 1: Elastic properties of overburden layers at seismic shot point A

Layer	V_p m/s	V_s m/s	V_p/V_s -	ρ kg/m^3	σ -	κ N/m^2 (x10^9)	μ N/m^2 (x10^9)	λ N/m^2 (x10^9)	E N/m^2 (x10^9)	Depth m	Lithology
1	803	305	2.633	1650	0.416	0.859	0.154	0.757	0.435	6.70	Unsaturated sand
2	1898	737	2.575	2045	0.411	5.886	1.111	5.145	3.135	11.9	Saturated tar sand
3	3300	1091	3.025	2349	0.439	21.55	2.796	19.98	8.044	-	Marl

Bima Journal of Science and Technology, Vol. 8(3) Sept, 2024 ISSN: 2536-6041

DOI: 10.56892/bima.v8i3A.802

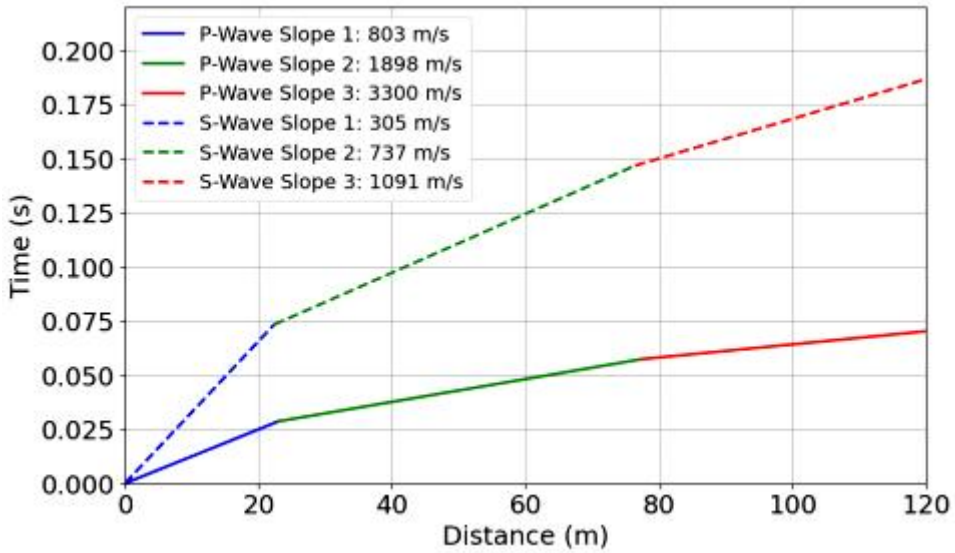

Figure 2: Traveltime-offset plot for seismic shot point A.

As can be seen in Figure 2, this layer has a primary wave velocity (V_p) of 803 meters per second and a secondary wave velocity (V_s) of 305 meters per second, giving a $\frac{V_p}{V_s}$ ratio of 2.633. The density is relatively low at 1650 kg/m^3. Its elastic properties include a Poisson's ratio of 0.416, indicating how much the material can deform. The bulk modulus, which measures resistance to uniform compression, is 0.859 x 10^9 N/m^2. The shear modulus, reflecting the material's response to shear stress, is 0.154 x 10^9 N/m^2. The Lame constant and Young's modulus are 0.757 x 10^9 N/m^2 and 0.435 x 10^9 N/m^2, respectively. These values suggest that this layer is quite loose and easily deformed.

Below the unsaturated sand, there is a layer of saturated tar sand extending down to 11.9 meters. This layer has a much higher primary wave velocity of 1898 m/s^2 and a secondary wave velocity of 737 m/s^2, resulting in a $\frac{V_p}{V_s}$ ratio of 2.575. The density here increases to 2045 kg/m^3, indicating the presence of pore-filling fluids. The Poisson's ratio is 0.411. The bulk modulus rises significantly to 5.886 x 10^9 N/m^2, indicating greater resistance to compression. The shear modulus is 1.111 x 10^9 N/m^2, and the Lame constant is 5.145 x 10^9 N/m^2. The Young's modulus for this layer is 3.135 x 10^9 N/m^2, suggesting this layer is more cohesive and stiffer than the unsaturated sand above. The third layer, composed of marl, extends further down but the depth is not specified. This layer shows the highest primary wave velocity at 3300 m/s^2 and a secondary wave velocity of 1091 m/s^2, resulting in a $\frac{V_p}{V_s}$ ratio of 3.025. The marl has the highest density at 2349 kg/m^3. Its Poisson's ratio is 0.439, slightly higher than the previous layers. The bulk modulus is 21.55 x 10^9 N/m^2, which indicate substantial resistance to compression. The shear modulus is 2.796 x 10^9 N/m^2, while the Lame constant and Young's modulus are 19.98 x 10^9 N/m^2 and 8.044 x 10^9 N/m^2, respectively. These high values indicate that the marl layer is very dense, rigid, and resistant to deformation.

Table 2 presents elastic parameters for three distinct subsurface layers identified at seismic shot point B. Each layer is characterized by its specific depth and various elastic properties. The first layer, identified as unsaturated sand, exhibits a P-wave velocity of 702 m/s and an S-wave velocity of 284 m/s (Figure 3), resulting in a $\frac{V_p}{V_s}$ ratio of 2.472.

Bima Journal of Science and Technology, Vol. 8(3) Sept, 2024 ISSN: 2536-6041

DOI: 10.56892/bima.v8i3A.802

Table 2: Elastic properties of overburden layers at seismic shot point B.

Layer	V_p	V_s	V_p/V_s	ρ	σ	κ	μ	λ	E	Depth	Lithology
	m/s	m/s	-	kg/m³	-	N/m² (x10⁹)	N/m² (x10⁹)	N/m² (x10⁹)	N/m² (x10⁹)	m	
1	702	284	2.472	1596	0.402	0.615	0.129	0.529	0.361	4.740	Unsaturated sand
2	1462	493	2.966	1917	0.435	3.565	0.466	3.255	1.338	10.22	Saturated tar sand
3	2545	830	3.066	2202	1.517	12.24	1.517	11.23	4.370	-	Marl

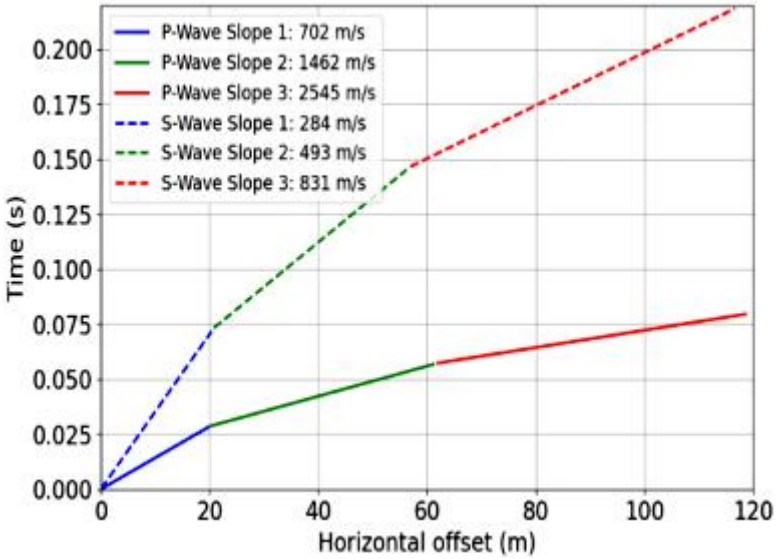

Figure 3: The plot traveltime-offset for seismic shot point A.

This layer has a density of 1596 kg/m³. The elastic moduli for this layer are relatively low, with a Lamé's first parameter of 0.402 x 10⁹ N/m², a shear modulus of 0.615 x 10⁹ N/m², a bulk modulus of 0.129 x 10⁹ N/m², a Young's modulus of 0.529 x 10⁹ N/m², and a Poisson's ratio of 0.361. These values indicate the loose and unconsolidated nature of unsaturated sand, which typically exhibits lower velocities and moduli due to its high porosity and lack of cementation. The second layer, composed of saturated tar sand, shows significantly higher values. The P-wave velocity is 1462 m/s, while the S-wave velocity is 493 m/s, giving a $\frac{V_p}{V_s}$ ratio of 2.966.

The density of this layer is 1917 kg/m³. The elastic moduli indicate a much stiffer and more consolidated material compared to the first layer, with Lamé's parameter at 3.565 x 10⁹ N/m², shear modulus at 3.255 x 10⁹ N/m², bulk modulus at 0.466 x 10⁹ N/m², Young's modulus at 10.22 x 10⁹ N/m², and Poisson's ratio at 1.338. These higher values are indicative of the presence of tar and saturation, which increase the rigidity and density of the layer, thereby enhancing its ability to transmit seismic waves. The third layer, which is marl, presents the highest values among the three layers. The P-wave velocity is 2545 m/s, and the S-wave velocity is 830 m/s, resulting in a $\frac{V_p}{V_s}$ ratio of 3.066. This layer has a density of 2202 kg/m³. The elastic moduli are significantly elevated, with Lamé's parameter at 12.24 x 10⁹ N/m², shear modulus at 11.23 x 10⁹ N/m², bulk modulus at 1.517 x 10⁹ N/m², Young's modulus

DOI: 10.56892/bima.v8i3A.802

at 4.370 x 10^9 N/m², suggesting the highly consolidated and cemented nature of marl. This layer's high velocities and moduli indicate a dense, rigid material capable of efficiently transmitting both P-waves and S-waves. As depth increases from the unsaturated sand to the saturated tar sand and finally to the marl layer, both wave velocities and elastic moduli significantly rise. This progression indicates the transition from loose, unconsolidated material to more dense and rigid geological formations, illustrating the varying seismic properties of these different lithologies.

Table 3: Elastic properties of overburden layers at seismic shot point C

Layer	V_p m/s	V_s m/s	V_p/V_s -	ρ kg/m³	σ -	κ N/m² (x10^9)	μ N/m² (x10^9)	λ N/m² (x10^9)	E N/m² (x10^9)	Depth m	Lithology
1	714	355	2.011	1602	0.253	0.547	0.202	0.413	0.507	6.16	Unsaturated sand
2	1522	697	2.184	1936	0.367	3.227	0.941	2.604	2.571	10.76	Clay
3	2817	1076	2.618	2258	0.415	14.43	2.614	12.68	7.356	-	Marl

Table 3 shows the elastic properties and velocities of the overburden layers at seismic shot point C. These parameters are crucial in determining the type of lithology present in the subsurface, which is a common practice in geophysics. The first layer has a P-wave velocity of 714 m/s and an S-wave velocity of 355 m/s (Figure 4), resulting in a ratio $\frac{V_p}{V_s}$ of 2.011. The density of this layer is 1602 kg/m³, and it exhibits a Poisson's ratio of 0.253. The bulk modulus is 0.547 x 10^9 N/m², the shear modulus is 0.202 x 10^9 N/m², the Lame constant is 0.413 x 10^9 N/m², and the Young's modulus is 0.507 x 10^9 N/m². The depth of this layer is 6.16 meters. These properties indicate that the layer is composed of unsaturated sand. The relatively low velocities of P-waves and S-waves, along with the elastic properties, suggest a loose, unconsolidated material, typical of unsaturated sand. The second layer has significantly higher velocities, with a P-wave velocity of 1522 m/s and an S-wave velocity of 697 m/s, leading to a $\frac{V_p}{V_s}$ ratio of 2.184. The density of this layer is 1936 kg/m³, and it has a Poisson's ratio of 0.367. The bulk modulus is 3.227 x 10^9 N/m², the shear modulus is 0.941 x 10^9 N/m², the Lame constant is 2.604 x 10^9 N/m², and the Young's modulus is 2.571 x 10^9 N/m². The depth of this layer is 10.76 meters. These properties suggest that the layer is composed of clay. The higher velocities and increased density compared to the first layer indicate a more consolidated material, characteristic of clay.

The third layer has the highest velocities among the three, with a P-wave velocity of 2817 m/s and an S-wave velocity of 1076 m/s, resulting in a $\frac{V_p}{V_s}$ ratio of 2.618. The density is 2258 kg/m³, and the Poisson's ratio is 0.415. The bulk modulus is 14.43 x 10^9 N/m², the shear modulus is 2.614 x 10^9 N/m², the Lame constant is 12.68 x 10^9 N/m², and the Young's modulus is 7.356 x 10^9 N/m². The depth of this layer is not specified. These properties are indicative of marl, a more consolidated and dense material compared to the previous layers. The high velocities and elastic moduli reflect the increased stiffness and rigidity typical of marl.

Bima Journal of Science and Technology, Vol. 8(3) Sept, 2024 ISSN: 2536-6041

DOI: 10.56892/bima.v8i3A.802

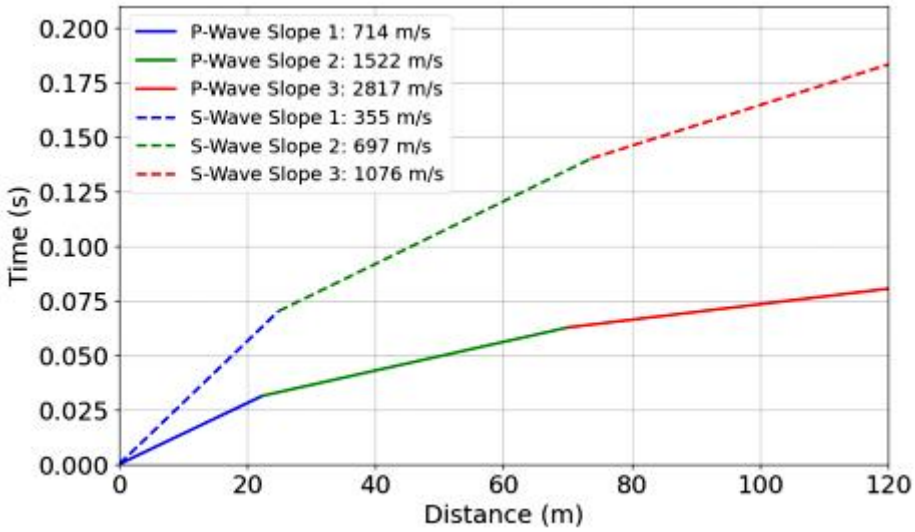

Figure 4: Traveltime-offset plot for seismic shot point C.

For seismic shot point D, the first layer, as shown in Table 4 and Figure 5, has a primary wave velocity of 787 m/s and a secondary wave velocity of 395 m/s, resulting in a $\frac{V_p}{V_s}$ ratio of 1.992. This ratio is typical for sand, especially when it is unsaturated. The density of this layer is 1640 kg/m³, which aligns with the expected range for sandy materials. The Poisson's ratio is 0.500, indicating a high degree of porosity, common in unsaturated sands. The elastic moduli - Young's modulus (0.673 x 10^9 N/m²), shear modulus (0.256 x 10^9 N/m²), and bulk modulus (0.504 x 10^9 N/m²) suggest that this layer is relatively soft and unconsolidated.

Table 4: Elastic properties of overburden layers at seismic shot point D.

Layer	V_p m/s	V_s m/s	V_p/V_s -	ρ kg/m³	σ -	κ N/m² (x10^9)	μ N/m² (x10^9)	λ N/m² (x10^9)	E N/m² (x10^9)	Depth m	Lithology
1	787	395	1.992	1640	0.500	0.673	0.256	0.504	0.780	5.42	unsaturated sand
2	1488	796	1.869	1925	0.299	2.600	1.219	1.823	3.129	11.20	Saturated tar sand
3	2457	1068	2.298	2180	0.382	9.867	2.491	8.178	9.162	-	Clay

The depth of this layer is 5.42 meters. The second layer in Table 4 has a primary wave velocity of 1488 m/s and a secondary wave velocity of 796 m/s, resulting in a $\frac{V_p}{V_s}$ ratio of 1.869. This ratio is indicative of saturated materials, where the presence of fluid (such as tar) within the pore spaces lowers the secondary wave relative to primary wave. The density is higher than the first layer at 1925 kg/m³, which is consistent with saturated conditions where the pores are filled with denser fluids. The Poisson's ratio of 0.299 is typical for saturated sand or tar sand, indicating moderate incompressibility. As can be seen in Table 4, the elastic moduli are higher than those of the first layer, suggesting increased rigidity due to saturation. The depth of this layer is 11.20 meters.

Bima Journal of Science and Technology, Vol. 8(3) Sept, 2024 ISSN: 2536-6041

DOI: 10.56892/bima.v8i3A.802

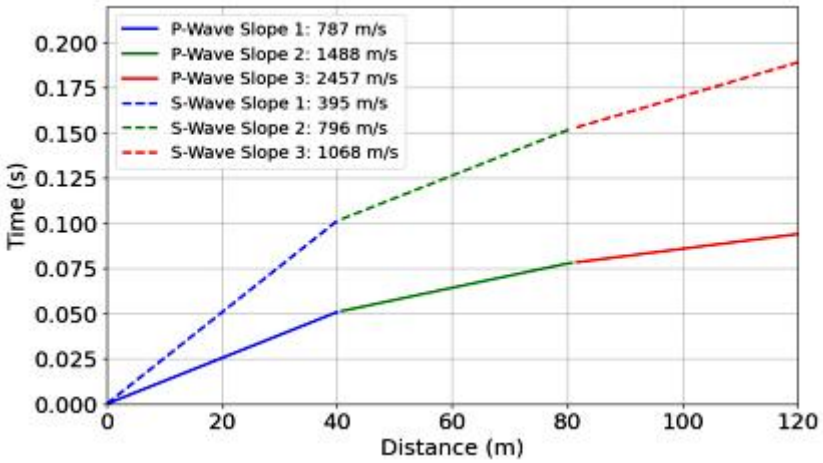

Figure 5: Traveltime-offset plot for seismic shot point D.

For the third, the primary wave velocity is 2457 m/s, and the secondary wave velocity is 1068 m/s, leading to a $\frac{V_p}{V_s}$ ratio of 2.298. This higher $\frac{V_p}{V_s}$ ratio is characteristic of clay, which tends to have a lower secondary wave due to its fine-grained and cohesive nature. The density of this layer is 2180 kg/m³, which is typical for clay materials. The Poisson's ratio is 0.382, indicating the relatively high compressibility of clay compared to sand. The elastic moduli suggest that the material is stiff and compact. Although the depth of this layer cannot be determined due to limitations in the methods used, the elastic properties strongly suggest it is clay. Based on the calculated seismic parameters, the lithology section for the study area was produced, as shown in Figure 6. Comparing the results from the four seismic stations, it can be seen that the lithology compositions of the study areas at different locations are similar, with slight variations in the thickness of the layers

.

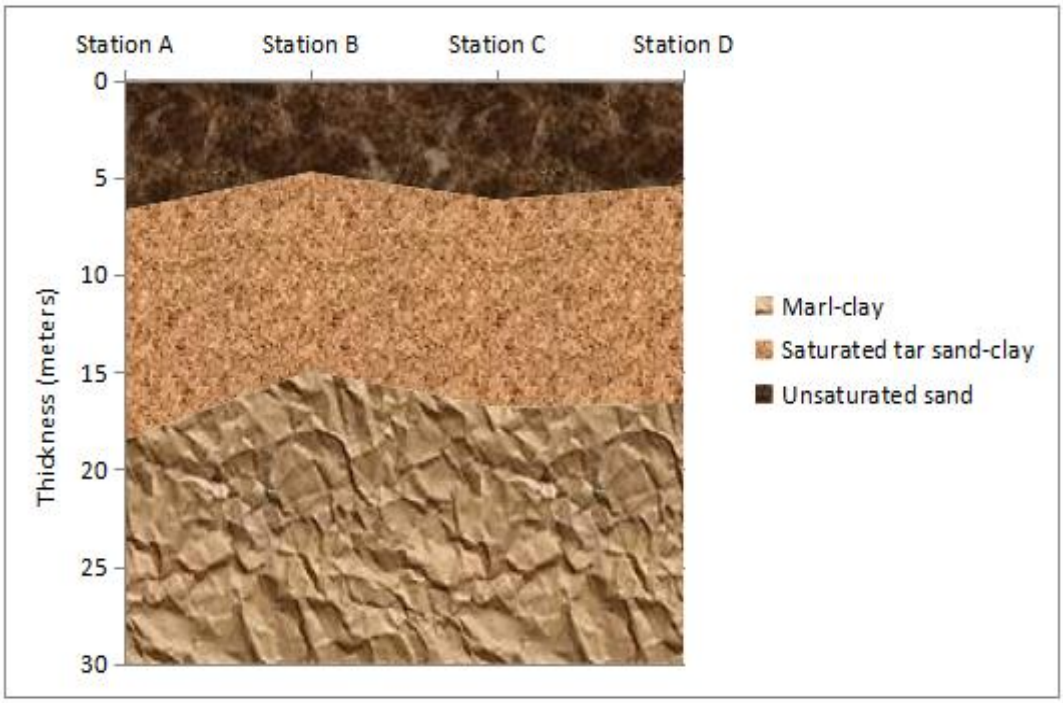

Figure 6: Lithology section of the study area.

DOI: 10.56892/bima.v8i3A.802

CONCLUSION

The seismic refraction survey conducted in Ayede, South-Western Nigeria, provided detailed information on the subsurface structure, revealing three primary layers: unsaturated sand, saturated tar sand, and marl/clay. Analysis of vertical component velocity data through the V_p/V_s ratio allowed for the accurate determination of elastic properties and the calculation of formation depths and thicknesses. Results indicate a progressive increase in both wave velocities and elastic moduli with depth. Economically, the identified clay deposits have potential uses in the production of drainage pipes, tiles, bricks, ceramics, pharmaceuticals, and as a cement filler. The marl may be suitable for fertilizer production, while the tar sand can be employed in road consolidation, foundation reinforcement, hydraulic fracturing, and glass manufacturing.

However, the study faced limitations due to the seismic source's energy capacity, which restricted depth penetration and resolution of small-scale heterogeneities. Variability in data quality was influenced by surface conditions such as vegetation and weather. Future research should incorporate higher energy sources and advanced seismic techniques, such as 3D seismic refraction or seismic tomography, and integrate other geophysical methods like ground-penetrating radar (GPR) or electrical resistivity tomography (ERT). Longitudinal studies and site-specific calibration models are recommended to enhance accuracy and address temporal variations in subsurface properties. Comprehensive environmental impact assessments and community engagement should precede extensive resource extraction to ensure sustainable utilization

REFERENCES

Abd El Aal, A. K., & Rouaiguia, A. (2020). Determination of the geotechnical parameters of soils behavior for safe future urban development, Najran Area, Saudi Arabia: implications for settlements mitigation. *Geotechnical and Geological Engineering*, *38*(1), 695-712.

Adamolekun, O. J., Busch, B., Suess, M. P., Molenaar, N., & Hilgers, C. (2022). Petrography and reservoir quality controls in shallow transitional marine Cretaceous-Paleogene deposits in the Dahomey Basin, Nigeria. *Journal of African Earth Sciences*, *186*, 104437.

Adediran, S. A., Adegoke, O. S., & Oshin, I. O. (1991). The continental sediments of the Nigerian Coastal Basins. *Journal of African Earth Sciences (and the Middle East)*, *12*(1-2), 79-84.

Adewoyin, O. O., Joshua, E. O., Akinyemi, M. L., Omeje, M., & Adagunodo, T. A. (2021). Evaluation of geotechnical parameters of reclaimed land from near-surface seismic refraction method. *Heliyon*, *7*(4).

Aisyah, R. R., Yulianita, D., Wafi, A., Setiawan, N. S., & Mariyanto, M. (2022, July). Application of seismic refraction method to identify rock layers around the lake body in Jakarta, Indonesia. In *Journal of Physics: Conference Series*, 2309(1), 012018).

Ajayi, O., Konwea, C. I., & Sodeinde, P. O. (2022). Groundwater Potential Assessment of the Sedimentary and Basement Complex Rocks of Ogun State, Southwestern Nigeria. *Journal of Water and Environment Technology*, *20*(6), 248-260.

Akingboye, A. S., & Ogunyele, A. C. (2019). Insight into seismic refraction and electrical resistivity tomography techniques in subsurface investigations. *Rudarsko-geološko-naftni Zbornik*, *34*(1).

Alabi, A. A., Lawal, R., Hamzat, K., Olaoye, A. M., Ogungbe, A. S., & Coker, J. O. (2023). Geophysical and

DOI: 10.56892/bima.v8i3A.802

Geotechnical Investigations of the Subsurface for Construction Purposes at Federal College of Education Osiele, Abeokuta, Southwestern Nigeria. *Nigerian Journal of Theoretical and Environmental Physics*, *1*(1), 9-21.

Alaminiokuma, G. I. (2020). Comparative analyses of uphole and seismic refraction techniques in near-surface attributes delineation: A case study of North-Central Niger Delta. *Geosciences*, *10*(1), 1-9.

Alhassan, D. U., Dangana, L. M., Salako, K. A., Jonah, S. A., & Ofor, N. P. (2010). Seismic refraction investigation of the subsurface structure at the southern part of Niger State College of Education, Minna, Nigeria. *Bayero Journal of Pure and Applied Sciences*, *3*(2), 56-61.

Balogun, O. B., Agbonjaru, D. C., & Ayolabi, E. A. (2023). Site investigation of soil competence by electrical resistivity and refraction seismic methods at a proposed building—a case study from Nigeria. *Arabian Journal of Geosciences*, *16*(7), 409.

Brixová, B., Mosná, A., & Putiška, R. (2018). Applications of shallow seismic refraction measurements in the Western Carpathians (Slovakia): case studies. *Contributions to Geophysics and Geodesy*, *48*(1), 1-21.

Çakır, Ö., & Coşkun, N. (2021). Theoretical issues with rayleigh surface waves and geoelectrical method used for the inversion of near surface geophysical structure. *Journal of Human, Earth, and Future*, *2*(3), 183-199.

Conway-White, O., Steelman, C. M., Smiarowski, A., Ugalde, H., Endres, A. L., Arnaud, E., & Parker, B. L. (2022). Improving spatial characterization of buried bedrock valleys through airborne frequency-domain electromagnetic, residual magnetic, and surface resistivity measurements. *Journal of Applied Geophysics*, *199*, 104584.

Cox, D. R., Newton, A. M., & Huuse, M. (2020). An introduction to seismic reflection data: Acquisition, processing and interpretation. In *Regional geology and tectonics* (pp. 571-603). Elsevier.

Crutchley, G. J., & Kopp, H. (2018). Reflection and refraction seismic methods. *Submarine geomorphology*, 43-62.

Eludoyin, A. O., Olusola, A., Fashae, O. A., Jeje, L. K., & Faniran, A. (2023). Geology and landscapes of the Southwestern Nigeria. *Landscapes and Landforms of Nigeria*, 201-216.

Fadhli, Z., Anda, S. T., Syukri, M., Karmel, M. E. R., Tutifla, A. S., Hasibuan, P., & Safitri, R. (2022). Ground Surface Quality Assessment Using P-wave Velocity from 2-D Seismic Refraction Method. *Aceh International Journal of Science and Technology*, *11*(3), 258-265.

Falowo, O. (2023). Subsoil Condition and Development of Geo-Data Set for Effective Design, Construction and Management of Engineering Structures in Ondo Metropolis, Southwestern Nigeria. *Malaysian Journal of Science and Advanced Technology*, 48-71.

Gago, P. A., Konstantinou, C., Biscontin, G., & King, P. (2022). A numerical characterisation of unconfined strength of weakly consolidated granular packs and its effect on fluid-driven fracture behaviour. *Rock Mechanics and Rock Engineering*, *55*(8), 4565-4575.

Griffiths, D. H., & King, R. F. (2013). *Applied geophysics for geologists and engineers: the elements of geophysical prospecting*. Elsevier.

Imani, P., Abd EL-Raouf, A., & Tian, G. (2021). Landslide investigation using Seismic Refraction Tomography method: a review. *Annals of Geophysics*, *64*(6), SE657-SE657.

Imani, P., Abd EL-Raouf, A., & Tian, G. (2021). Landslide investigation using

DOI: 10.56892/bima.v8i3A.802

Seismic Refraction Tomography method: a review. *Annals of Geophysics*, *64*(6), SE657-SE657.

Kaunda, R. B. (2021). Role of localized elevated pore pressures and strain localization mechanisms in slope stability problems. In *Modeling in Geotechnical Engineering* (pp. 183-203). Academic Press.

Kearey, P., Brooks, M., & Hill, I. (2002). *An introduction to geophysical exploration* (Vol. 4). John Wiley & Sons.

Malehmir, A., Socco, L. V., Bastani, M., Krawczyk, C. M., Pfaffhuber, A. A., Miller, R. D., ... & Dahlin, T. (2016). Near-surface geophysical characterization of areas prone to natural hazards: a review of the current and perspective on the future. *Advances in Geophysics*, *57*, 51-146.

Maunde, A., & Bassey, N. E. (2017). Seismic refraction investigation of fracture zones and bedrock configuration for geohydrologic and geotechnical studies in part of Nigeria's Capital City, Abuja. *Journal of Earth Sciences and Geotechnical Engineering*, *7*(2), 91-102.

Mengjia, Z., Guangzeng, W., Sanzhong, L., Yongjiang, L., Pengcheng, W., Lingli, G., ... & Taihai, S. (2024). An overview of structures associated with bends of strike-slip faults: Focus on analogue and numerical models. *Marine and Petroleum Geology*, 106983.

Mosuro, G. O., Adebisi, N. O., Ariyo, S. O., Omosanya, K. O., Bayewu, O. O., & Oloruntola, M. O. (2021). Redefining the boundary between crystalline and sedimentary rock of Eastern Dahomey Basin. *Scientific Reports*, *11*(1), 5016.

Nogueira, P. V., Rocha, M. P., Borges, W. R., Silva, A. M., & de Assis, L. M. (2016). Study of iron deposit using seismic refraction and resistivity in Carajás Mineral Province, Brazil. *Journal of Applied Geophysics*, *133*, 116-122

Nton, M. E., & Adeyemi, M. O. (2015). Petrography, compositional characteristics and stable isotope geochemistry of the Ewekoro formation from Ibese Corehole, eastern Dahomey basin, southwestern Nigeria. *Global Journal of Geological Sciences*, *13*, 35-52.

Nyquist, J. E., Doll, W. E., Davis, R. K., & Hopkins, R. A. (1996). Cokriging surface topography and seismic refraction data for bedrock topography. *Journal of Environmental and Engineering Geophysics*, *1*(1), 67-74.

Olusola, F. O. (2021). The Usefulness of Engineering Geological and Geotechnical Studies in Civil Engineering Sites Foundation Design Parameters Consideration and Construction: A Case Study in SW Nigeria. *International Journal of Earth Sciences Knowledge and Applications*, *3*(3), 173-189.

Oluwajana, O. A., Opatola, A. O., Adamolekun, O. J., Ndukwe, O. S., Olawuyi, G. T., Ofiwe, C. U., ... & Oluwajana, O. O. (2021). Sedimentation, depositional environments, and hydrocarbon potential of the Maastrichtian-Paleocene Araromi Formation, eastern Dahomey (Benin) Basin, southwestern Nigeria. *Journal of Petroleum Exploration and Production Technology*, *11*(11), 3917-3934.

Ozebo, V. C., & Ikuemonisan, F. E. (2019). Evaluation of allowable bearing capacity of Ayila Soil, south-west Nigeria. *Journal of Applied Sciences and Environmental Management*, *23*(4), 621-625.

Pegah, E., & Liu, H. (2016). Application of near-surface seismic refraction tomography and multichannel analysis of surface waves for geotechnical site characterizations: A case study. *Engineering Geology*, *208*, 100-113.

DOI: 10.56892/bima.v8i3A.802

Rana, S., Mishra, V. N., & Rai, P. K. (2023). Applications of Geophysics in Structural and Geotechnical Engineering. In *International Conference on Interdisciplinary Approaches in Civil Engineering for Sustainable Development* (pp. 323-334). Singapore: Springer Nature Singapore.

Reynolds, J. M. (2011). *An introduction to applied and environmental geophysics*. John Wiley & Sons.

Rucker, M. L. (2002). Seismic refraction interpretation with velocity gradient and depth of investigation. In *Proceedings of the Geophysics 2002 conference, April*, 15-19.

Sheriff, R. E., & Geldart, L. P. (1995). *Exploration seismology*. Cambridge university press.

Silahtar, A., Kanbur, M. Z., & Beyhan, G. (2020). Analysis of seismic site characterization of the Isparta basin (southwestern Turkey) using passive surface-wave method (ReMi™) and borehole data. *Journal of Earth System Science*, *129*, 1-21.

Sunkpal, D. T., Ankamah, A. T., Tuoyang, M. K., & Ankah, M. L. Y. (2022). Geophysical investigation of groundwater potential zones, and modeling of subsurface materials using seismic refraction surveys. *Modeling Earth Systems and Environment*, *8*(4), 4389-4400.

Syukri, M., Saad, R., & Fadhli, Z. (2020). Capability of P-and S-wave seismic refraction in delineating the Blang Bintang Sanitary Landfill (TPA) ground subsurface. *Songklanakarin J. Sci. Technol*, *42*, 780-787.

Tokgozoglu, K., Aladag, C. H., & Gokceoglu, C. (2023). Artificial neural networks to predict deformation modulus of rock masses considering overburden stress. *Geomechanics and Geoengineering*, *18*(1), 48-64.

Uecker, R. K., Flinchum, B. A., Holbrook, W. S., & Carr, B. J. (2023). Mapping bedrock topography: a seismic refraction survey and landscape analysis in the Laramie Range, Wyoming. *Frontiers in Water*, *5*, 1057725.

Uhlemann, S., Hagedorn, S., Dashwood, B., Maurer, H., Gunn, D., Dijkstra, T., & Chambers, J. (2016). Landslide characterization using P-and S-wave seismic refraction tomography—The importance of elastic moduli. *Journal of Applied Geophysics*, *134*, 64-76.

Ullah, F., Su, L., Alam, M., Cheng, L., & Kazantseva, E. S. (2023). Applications of remote sensing and near-surface geophysical methods for the investigations of a morainic ridge susceptible to landslide. A case study from the high lands of the Himalayas, Pakistan. *Journal of Applied Geophysics*, *217*, 105180.

Wang, H., Wu, S., Qi, X., & Chu, J. (2021). Modified refracted ray path method for determination of shear wave velocity profiles using seismic cone. *Engineering Geology*, *293*, 106330.

Washima, A., Anti, K., & Luper Tsenum, J. (2020). Advantages and Limitations of Seismic Refraction Method Using Hammer Sources. *ScienceOpen Preprints*.

Zhu, J., Li, W., & Liu, Y. (2022). Analysis of overburden deformation and migration under huge thick unconsolidated layers based on multiple approaches. *Minerals*, *12*(12), 1510.